# Tests of MVD Prototype Pad Detector with a $\beta^-$ Source

Sang Yeol Kim, Young Gook Kim, Sang Su Ryu, Ju Hwan Kang*

*Department of Physics, Yonsei University*

*134 Shinchon-dong Seodaemum-ku Seoul 120-749 South Korea*

**TEL. +82 2 361 2621 FAX. +82 2 392 1592 e-mail. jhkang@phya.yonsei.ac.kr*

Jehanne Simon-Gillo, John P. Sullivan, Hubert W. van Hecke

*Group P-25, MS H846, Los Alamos National Laboratory*

*Los Alamos, NM, 87545, USA*

and

Guanghua Xu

*Physics Department, University of California*

*Riverside, CA 92521*

## Abstract

The MVD group has been testing two versions of silicon pad detectors. One design uses a single metal layer for readout trace routing. The second type uses two layers of metal, allowing for greatly simplified signal routing. However, because the readout traces for the pads pass over the other pads in the same column (separated by an oxide layer), the double-metal design introduces crosstalk into the system. A simple test stand using a $^{90}$Sr $\beta^-$ source with scintillator triggers was made to estimate the crosstalk. The crosstalk between pads in the same column of the pad detector was 1.6 – 3.1%. The values measured between pads in different columns were very close to zero. The measured crosstalk was below our maximum allowed value of 7.8%.

## I. INTRODUCTION

The Relativistic Heavy-Ion Collider (RHIC) is a nucleus-nucleus collider being built at Brookhaven National Laboratory. It is capable of accelerating gold nuclei to 100 GeV/nucleon in each direction. PHENIX [1,2] is one of the four major experiments at RHIC that will look for experimental evidence of a phase transition to and from a quark-gluon plasma, a form of matter thought to have existed at the beginning of the Universe. The colliding beams are parallel to the axis of the Multiplicity Vertex Detector (MVD), which is in the center of the PHENIX experiment, surrounding the region where the two beams collide. The MVD includes silicon strip detectors arranged in two concentric barrels, with strips running perpendicular to the beam axis. The endcaps are an arrangement of silicon pad detectors and extend the range of angular distribution measurements. The MVD measures the charged-particle distribution event-by-event, provides event characterization and a centrality trigger to the PHENIX experiment. Simulations indicate that correlating the hits in the two-barrels allows one to determine the vertex of the collision in three dimensions with a several hundred micron resolution. The segmentation of the pad detectors also allows the study of fluctuations in charged particle multiplicity, a signature of the formation of a quark-gluon plasma. Details of the Multiplicity Vertex Detector are presented elsewhere [3–5].

The PHENIX MVD group has been testing two types of silicon pad detectors for the "endcaps" of the MVD [6] (see Fig. 1). One design, "single-metal", has traces which take the signals from the pads (i.e. the keystone shaped counting elements which collect the charge) to the edges of the detector wafers. To prevent the traces from crossing, they are brought to 3 of the 4 edges of the detector wafer. These traces are in the same metallic plane as the pads. The signals would be connected to the electronics via relatively complex cable which overlays the detector wafer, and routes all signals to the top of the detector. The "single metal" design is more conventional and is historically the technology employed in silicon detectors. The MVD would like to use the newer and more "cutting-edge" technology of the

"double metal" design. The "double metal" design has many advantages over the traditional "single metal" design: eliminates the need of a specialized kapton cable for readout, reduces the amount of wirebonding, facilitates detector probing, facilitates assembly and handling, therefore increasing yield, and allows for a sequential readout. The routing is much simpler if a "double-metal" detector design is used. In this design the traces which take the signals to the edge of the detector are separated from the pads by an oxide ($SiO_2$) layer [7]. The traces go from the pads, through the oxide layer, to a second "metal" layer. The signal traces can then all be brought to the top edge of the detector, eliminating the cable overlays of the single-metal design. However, there was some concern that the coupling through the capacitors formed by the traces from one pad crossing above the pads for other channels would introduce crosstalk into the system. In the study described here, we have measured the crosstalk in a prototype double-metal pad detector.

We established a limit on the amount of crosstalk which is acceptable by considering the effects of crosstalk of the pad detector trigger for central Au+Au events using a Monte Carlo simulation of the MVD with Hijing [8,9] events as input. The average occupancy of the pad detector pads in this case was $\approx 16\%$. The discriminator thresholds on each pad, used in the trigger, will be set at about 0.25 times the average signal from a minimum-ionizing particle (mip). There are 21 pads in each "column" of pads. A column is a set of pads at the same azimuthal angle, but different radial distances from the beam. The signal traces in the double metal design all run to the top (largest radial distance from the beam) edge of the pad detector. This means that the top pad has 20 signal traces crossing it and that the bottom pad's readout trace crosses over 20 other pads. If there is crosstalk between each pad in a column and the 20 other pads in the column, we would like the total crosstalk contribution to a pad without a hit to be small enough to avoid triggering the pad's discriminator. That is, we would like (occupancy=0.16)*(20 pads in column contributing to crosstalk)*(crosstalk)*(average signal per particle=1 mip) to be less than 0.25 mip. This gives a limit on the crosstalk of: crosstalk $< 0.25/(20*0.16) = 7.8\%$. Correction for crosstalk can be made in data analysis, but it is preferable to have a crosstalk level significantly below

this 7.8% limit.

## II. TEST STAND

### A. Description of the silicon pad detector

Figure 1 shows the layout of the silicon pad detector. It has 252 elements(21 rows and 12 columns), and the size of the pads increases from the inner to the outer radius of the wedge. The smallest element is 2.0mm $\times$ 2.0mm, and the largest is 4.5mm $\times$ 4.5mm. The detector is single-sided, ac-coupled with coupling capacitor values ranging from approximately 200 for the smallest element to 2000nF for the largest element. The dielectric oxide is 200nm thick. The detector is biased by polysilicon resistors whose average value is 5M$\Omega$. The bias resistors are distributed between alternate rows of the pads having a 300$\mu$m wide gap to connect to the upper and the lower pads. The gap between pads in adjacent columns is 200$\mu$m. The ratio of the area of the readout electrode to the area of the pad is kept roughly constant. The second metal is used to route the pad outputs to bond pads located at the outer most radius of the detector. A 4$\mu$m layer of silicon dioxide separates two metal layers [10]. Typical I/V characteristics of individual pads show nearly ideal diode behavior. The leakage current varies from about 400pA for the smallest pads, to about 1nA for the largest pads. From the C/V characteristics of individual pads, a full depletion around 30V was estimated. The pad capacitance at full depletion ranges from 3pF for the small pads to 10pF for the large ones [11].

### B. Cabling convention and front end electronics

BVX preamplifier [12] was used in this test. Figure 2 shows the block diagram of the BVX preamplifier. It utilizes a PMOS cascode amplification stage for low 1/f noise. The input device operates in a weak inversion with a drain current of 100$\mu$A. Versions of this design are presently being used by not only PHENIX, but also by the PHOBOS detector collaboration

[13](also at RHIC), and the Naval Research Laboratories(NRL) for Germanium spectroscopy [14]. The PHENIX version employs a wideband gain stage after the preamplifier. The circuit is fabricated in 1.2$\mu$m n-well CMOS and has an 85$\mu$m/channel pitch. In this design, the feedback capacitor is split into two parts, Cf1 and Cf2, as shown in figure 3. Capacitor Cf1 is connected from the input to the dominant node. The other capacitor Cf2 is connected from the input to a source follower output. The preamplifier has a dynamic range of 75fC which corresponds to a full scale output voltage of 1.5V and a signal range of 19 MIPs. The channel-channel crosstalk was measured and found to originate almost entirely from coupling between wirebonds on the inputs. Without wirebonds present, the crosstalk was found to be less than 1% [15,16].

Eight channels out of 252 channels were wire-bonded to the front-end electronics (FEE) since we used a FEE board containing a single BVX pre-amplifier chip with eight channels. Figure 4 shows the wire-bonded channels in this test and their respective cabling numbers to the FEE. The size of each readout pad is exaggerated. Channel 1,2,3 are 2.0mm $\times$ 2.0mm, channel 4,5 are 2.5mm $\times$ 2.5mm, channel 6 is 4.0mm $\times$ 4.0mm, and channel 7,8 are 4.5mm $\times$ 4.5mm respectively. Channel 1 through 5 sit in the same column and channel 6 through 8 are in the neighboring column. Therefore, the readout traces for channels 1–5 do not cross above the pads for channels 6–8 and vice-versa.

### C. Beta source

$^{90}$Sr has a half-life of 28.74 years. It beta decays to $^{90}$Y with a 546.2keV beta end point energy. $^{90}$Y is also unstable and decays to $^{90}$Zr with a half-life of 64.1 hours. All of the $^{90}$Sr decays to the ground state of $^{90}$Y. $^{90}$Y has a relatively complicated decay scheme but most decays are to the ground state of $^{90}$Zr with a small branching ratio to an excited state which can be ignored [17]. Figure 5 shows the complete double decay scheme of $^{90}$Sr. The source is small enough to be regarded as a point source and contained inside a brass cylinder thick enough to prevent beta particles from penetrating. The cylinder has a 1mm $\times$ 6mm

rectangular hole on the bottom side. The distance from the source to the hole is 40mm, so that only nearly vertical electrons to the silicon pad detector plane can pass the hole.

The electrons from the decays of $^{90}$Y to the ground state of $^{90}$Zr have its maximum kinetic energy of 2281.4keV. This is the electron used in the tests. The 64.1 hour half-life of $^{90}$Y is long enough to prevent accidental coincidences between beta particles from $^{90}$Zr and $^{90}$Y. A 2.28MeV electron has a range in Si around 5mm (5000$\mu$m). Using a Monte Carlo simulation, we have checked that the high energy portion of the electrons from $^{90}$Y can mimic the energy loss of a minimum ionizing particle in the silicon pad detector.

### D. Triggering scintillators and the test stand geometry

Although electrons from $^{90}$Sr can penetrate all the elements including the silicon detector, its supporting material, and the two scintillation fibers, their energy is still not high enough to be free from a large angle deflection when they pass through materials. There is spurious crosstalk due to this beta particle deflection effect, and for the accurate crosstalk measurement it is necessary to select only the electrons which penetrate the silicon pad detector with a small deflection angle. Figure 6 shows our test stand geometry. The triggering scintillators are composed of two 2mm $\times$ 2mm $\times$ 25mm scintillating fibers and a 25mm $\times$ 25mm $\times$ 12.5mm plastic scintillator. Two fibers are configured as an "X" and they define the narrow incident angle of beta rays into an $\approx$ 2mm $\times$ 2mm square. The plastic scintillator which is beneath the scintillation fibers is to discriminate against low energy beta particles which are more likely deflected into the large angle. This bottom scintillator is thick enough to stop any incident beta particles from the $^{90}$Sr source.

The silicon pad detector is placed 25mm above the uppermost scintillation detector. The silicon pad detector is supported by a 2mm thick G10 circuit board, and the detector together with circuit board and FEE board are attached to the 15mm aluminum support. There are holes in the aluminum support around the tested silicon readout pads to avoid beta particle being absorbed by the thick aluminum support. The high energy portion of the

electrons from the beta source have sufficient range to pass through the 300$\mu$m silicon pad detector, the 2mm G10 circuit board, the two scintillating fibers, and then stop somewhere in the thick bottom plastic scintillator. The source is positioned 20mm above the silicon detector. There is no collimator except the hole on the brass source container.

All of the detectors and the source assembly are placed in a dark box, and the electronics, with the exception of the BVX preamplifier, are placed outside the dark box. The electronics are composed of NIM amplifiers, discriminators, coincidence units, and CAMAC digitizers. Because the BVX preamplifier is DC coupled, it is necessary to insert a capacitor between the preamplifier and the main NIM amplifier to measure the AC coupled signal. VME combined with a CAMAC system was used to read out the data.

## III. MONTE CARLO SIMULATIONS

The purpose of the Monte Carlo simulation is to estimate the level of spurious crosstalk from the deflected beta particles and the relative counting rate of the test system. A beta particle can hit one channel of the pad detector(referred to here as a "primary channel"), followed by deflection, then hit a neighboring channel. This also is observed as crosstalk. It is necessary to estimate the level of such spurious crosstalk for the measurement of the real crosstalk in the silicon detector itself.

The GEANT code [18] was used in the simulation study. The cascaded decays of $^{90}$Sr and $^{90}$Y were simulated including the small branching ratio to the excited state of $^{90}$Zr. Simple flat distributions from zero to the end point energy were used as both $^{90}$Sr and $^{90}$Y energy spectra. Figure 7 shows some results of the GEANT simulation. The beta particles from the $^{90}$Sr source undergo significant deflection in the test setup. Table 1 shows the simulation result for the case of requiring two scintillating fibers for the trigger. The efficiency is defined as the ratio of electrons passing the trigger to electrons coming out of the source container. This trigger imposes a severe constraint on the incident angle due to the small overlap area(2mm $\times$ 2mm) of the two fibers. Unfortunately, this restriction

degrades the counting efficiency. Among beta particles emerging from the source container, only $4.5\times10^{-5}$ satisfy the trigger condition in the smallest pad channel. For large pads this fraction increases slightly to $1.6\times10^{-4}$. As can be seen in figure 7, the small efficiency is caused by multiple scattering of electrons, as well as by the ranging-out effect.

The simulation was repeated with the two scintillating fibers removed from the trigger condition in order to increase the counting efficiency. The trigger condition is then only simultaneous hits in the primary silicon channel and the plastic scintillator. Table 2 shows the results of this simulation. The efficiency was increased by more than a factor of 100. The spurious crosstalk in the neighboring channels is 0.19% and 0.09% in the 2.0mm $\times$ 2.0mm and 4.5mm $\times$ 4.5mm pad channels respectively. There was no spurious crosstalk between non-neighboring channels in any case.

## IV. MEASUREMENT

### A. Calibration

The external electronics outside the dark box were calibrated using a pulse generator. The same pulses were fed into the circuit just after the preamplifier. Using this calibration procedure, the external amplifier gains and the ADC slopes were obtained. In the next calibration step, the gain of the individual silicon pad detector plus the BVX preamplifier was measured. Beta particles were used to mimic minimum ionizing particles. ADC distributions for minimum ionizing particles were measured for each channel of the silicon pad detector. Table 3 shows the relative gains of the silicon pad detector plus BVX preamplifier for the eight channels used in the test. Gains for the pad detector and the preamplifier were not measured separately to avoid re-wirebonding the detector to front end electronics.

### B. Setup

For the trigger using only the plastic scintillator and the primary pad channel, the simulation study showed the spurious crosstalk levels due to the electron scattering to be only 0.14% in the neighboring channel and 0.02% in the next neighboring channel. The discriminator thresholds for these two detectors were set just above the noise level. Figure 8 shows the block diagram of the electronics for the crosstalk measurement. The coincidence unit was set to have $1\mu$s resolving time. The accidental coincidence rate was checked by observing the timing pulses in a digital oscilloscope. No random timing fluctuation between the scintillator pulse and the pulse from the silicon pad detector was observed. This corresponded to the estimation of the accidental coincidence rate in our setup to be $1/\tau A\epsilon \approx 10^{-4}$, where $\tau$, A and $\epsilon$ represent the coincidence resolving time, the source strength and the counting efficiency respectively. This can be checked by looking at the ADC distribution of the primary channel(figure 9A). A high energy tail originating from the random coincidence of low energy electrons would show up as in figure 9(A) for the ADC distribution without trigger.

Simple amplifiers without any pulse shaping were used just to amplify the small signals from the preamplifiers because the preamplifier already shaped the pulse from the silicon detector. The preamplifier output has a risetime of 200ns. AC-coupling capacitors were inserted to remove the DC offsets from the silicon detector. Because our test system was relatively noisy and did not have any filtering device, the random noise level was expected to be larger or comparable to the crosstalk signal. Charge sensing ADCs(LeCroy 2249W) with $1\mu$s gate width were used to integrate all the crosstalk signal and noise.

### C. Analysis and results

After illuminating one pad detector channel with the beta source, the eight wirebonded channels of the silicon detector were read out simultaneously. For each channel, 20,000

counts of data were taken with the pad detector being aligned with the source and the trigger counter. The same amount of data was taken after dislocating the pad detector from the electron path. The former data was for the crosstalk and the random noise, and the latter was for the random noise only. Thus the pure crosstalk level can be obtained after subtracting the latter data from the former one. This procedure was repeated for all eight silicon channels.

Figure 9 shows some sample of ADC distributions which was obtained after subtracting the "source off" data from the "source on" data. Figure 9A shows the ADC distribution of the primary pad channel for all signals passing its own discriminator cut and 9B shows a typical Landau distribution for the primary channel obtained after imposing the trigger condition utilizing the scintillator. The narrow peak near zero in figure 9A represents the noise distribution. Figure 9C shows the ADC distributions of the channels in the same column with the primary channel. Because the "source on" and the "source off" data were taken separately and thus completely uncorrelated with each other, the width of this distribution is mainly caused by noise distribution of "source on" and "source off" data. The individual noise level in table 4 was obtained by looking at ADC values in the "source off" data. The deviation of the mean value of the distribution in figure 9C and 9D from zero represents the crosstalk. As one can see in figure 9D, this shift was strikingly decreased in the channel of the different column from the primary channel.

The measurement showed that the crosstalk occurs along channels in the same column on which the read out traces run, and very small crosstalk occurs along the channels in the different column. The amount of the crosstalk levels in the small-sized pad channels (2.0mm $\times$ 2.0mm and 2.5mm $\times$ 2.5mm) were 2.1% in average when one of the small channels was chosen as a primary channel and 2.8% in average in the large-sized channels (4.0mm $\times$ 4.0mm and 4.5mm $\times$ 4.5mm) when one of the large channels was the primary channel. The crosstalk is bi-directional within a column. That is, the crosstalk between a pad near the bottom whose signal line crosses a pad above it in the same column is about the same when either of the pads is selected as the primary pad. Table 4 shows the results of crosstalk measurements for

8 wirebonded channels along with the noise levels of the primary channels. Except for the case of channel 2 which showed relatively large crosstalk levels, all the channels in different columns (channel #6, #7, and #8) showed crosstalk less than 1%(0.2% in average) when the small-sized pad channels were illuminated. When the large channels were illuminated, the small-sized channels in the different column exhibited the negative crosstalk without exception (-0.6% in average).

The crosstalk may not be due to the electronic interference between the readout traces. If this is the case, the level of crosstalk would change depending on the relative position of the readout traces, and a larger value of crosstalk is expected between adjacent traces than that of nonadjacent traces. The measurement does not show such dependency. The crosstalk is thought to be caused by the capacitance coupling between the pad silicon and the metal readout trace which runs over it. In this case the crosstalk would be observed between the pads in the same column but would not be observed between the pads in different columns because readout traces run over only pads in the same column. Figure 10 shows some of the results graphically. Here the arrows represent the primary channels. As one can see in the figure there are clear patterns of the crosstalk: bi-directional in the same column and no major crosstalk in the different column.

The ratio of the crosstalk to the pad area could be understood by the simple model. The pad silicon and the metal readout trace which are separated by 4$\mu$m thick silicon dioxide acts a kind of capacitor. Its capacitance is proportional to the overlapping area between the pad silicon and metal trace, and inversely proportional to the distance between two metals. Because the width of the readout trace is the same for all pads, the above area is proportional to the length of the silicon pad. If the thickness of the insulating silicon dioxide layer is homogeneous, the capacitance is proportional to the length of the pad. Thus the crosstalk in the large pads is expected to be roughly two times bigger than that in the small pads. The measured value shows that the crosstalk level in the large pads is roughly 1.5 times of that in the small pads. The discrepancy can be explained if we consider the effect of the minor crosstalk. The reason of the minor crosstalk is not clear. If we assume that it does

not depend on the capacitance coupling between the silicon pad and the readout trace, the same amount of the minor crosstalk which was measured at the different column would be contained in the crosstalk measured at the same column. This is 0.5% in average including the noisy #2 channel when one of the small channel is a primary channel and -0.6% when one of the large channel is a primary channel. By subtracting this minor crosstalk effect, the net crosstalk due to the capacitance coupling can be obtained. The average crosstalk value is 1.6% in the small pads and 3.4% in the large pads, which corresponds to the relative size of the large and the small pads. These values correspond to those of the previous measurements using an infrared laser station, in which the measured crosstalk values include those from pickup from the logic edge that fires the laser and positioning motor signals [11].

## V. SUMMARY

A simple test stand for the crosstalk measurement of the silicon pad detector was made using a $^{90}$Sr beta source and plastic scintillators. The Monte Carlo simulation study showed beta particles from the $^{90}$Sr can mimic a minimum ionizing particle in such a test. The simulations also showed that the effect of the spurious crosstalk level by scattered electrons is negligible in the crosstalk measurement.

The measurements determined that the crosstalk level is 1.6% – 3.1%, which does not exceed our maximum allowed level of 7.8%. This proved the double-metal silicon pad detector can be used as a PHENIX MVD detector component. The major crosstalk occurred between the pair of pads in the same column – any pair of pads for which the readout trace of one pad crosses the other pad exhibits crosstalk – but not between different columns. The major crosstalk can be understood as a consequence of the capacitance coupling between the pad silicon and the metal readout trace that runs over it, showing that the relative amount of the measured crosstalks corresponds to the relative size of the pads.

## VI. ACKNOWLEDGEMENTS

This work was performed at Los Alamos National Laboratory and supported in part by the Korea Research Foundation (1997-001-D00118). The MVD project is supported by the United States Department of Energy.

# REFERENCES


[1] PHENIX Conceptual Design Report, Brookhaven National Laboratory, 1993.

[2] D.P. Morrison for the PHENIX Collaboration, Proceedings of the Thirteenth International Conference on Ultra-Relativistic Nucleus-Nucleus Collisions, Tsukuba, Japan, December 1-5, 1997.

[3] J.S. Lock *et al.* Nucl. Instr. and Meth. **A345** (1994) 284.

[4] J.S. Kapustinsky *et al.* Nucl. Instr. and Meth. **A392** (1997) 192.

[5] E. Bosze *et al.* Nucl. Instr. and Meth. **A400** (1997) 224.

[6] D. Jaffe *et. al.* Nucl. Instr. and Meth. submitted on February 12(1998).

[7] J.S. Kapustinsky *et. al.* Nucl. Instr. and Meth. **A409** (1998) 173.

[8] M. Gyulassy, X.-N. Wang, Phys. Commun. **83** (1994) 307.

[9] X.-N. Wang, M. Gyulassy, Phys. Rev. **D44** (1991) 3501.

[10] C.L. Britton *et. al.* IEEE Transactions on Nuclear Science. **41** (1994) 352.

[11] J. Kapustinsky *et. al.* Nucl. Instr. and Meth. **A329** (1997) 192.

[12] J.S. Kapustinsky *et. al.* Proceedings of the Frontier Detectors for Frontier Physics Conference, La Biodla, Isola d'Elbar, Italy, May 25-31, 1997.

[13] M. Plesko and B. Wadsworth, *MIT-LNS Electronics Facility*, Tech. Note 94-8, August 1994.

[14] R.A. Kroeger *et. al.* IEEE Trans. Nucl. Sci., **42** (1995) 921.

[15] C.L. Britton *et. al.* Proceedings of the First Workshop on Electronics for LHC Experiments, Lisbon, Portugal, September 11-15, 1995.

[16] C.L. Britton *et. al.* IEEE Trans. Nucl. Sci., **44** (1997) 283.

[17] R.B. Firestone and V.S. Shirley, *Tables of Isotopes*, 8th ed.(Wiley, New York, 1996).

[18] *GEANT manual*, CERN program library long writeup W5013(1993).

## TABLES

TABLE I. The Monte Carlo simulation results when the X shaped scintillation fibers are included in the trigger condition.

| | | |
|---|---|---|
| primary channel | #1(2.0mm × 2.0mm) | #8(4.5mm × 4.5mm) |
| crosstalk | 0.00%(in channel #2) | 0.00%(in channel #7) |
| crosstalk | 0.00%(in channel #3) | 0.00%(in channel #6) |
| efficiency | $4.5 \times 10^{-5}$ | $1.6 \times 10^{-4}$ |

TABLE II. The Monte Carlo simulation results when the X shaped scintillation fibers are excluded in the trigger condition.

| | | |
|---|---|---|
| primary channel | #1(2.0mm × 2.0mm) | #8(4.5mm × 4.5mm) |
| crosstalk | 0.19%(in channel #2) | 0.09%(in channel #7) |
| crosstalk | 0.00%(in channel #3) | 0.00%(in channel #6) |
| efficiency | $6.2 \times 10^{-3}$ | $1.9 \times 10^{-2}$ |

TABLE III. The relative gain of the silicon pad detector + BVX preamplifier.

| channel number | relative gain | channel number | relative gain |
|---|---|---|---|
| 1 | 1.000 ± 0.003 | 5 | 1.033 ± 0.004 |
| 2 | 1.050 ± 0.004 | 6 | 1.003 ± 0.004 |
| 3 | 0.990 ± 0.004 | 7 | 0.925 ± 0.004 |
| 4 | 1.020 ± 0.004 | 8 | 0.951 ± 0.004 |

TABLE IV. The noise level of the silicon pad detector. "Noise" is defined as the rms width of the ADC (pedestal) distribution with no source pointed at the channel.

| channel number | noise/1MIP(%) | channel number | noise/1MIP(%) |
|---|---|---|---|
| 1 | 3.49 ± 0.01 | 5 | 3.63 ± 0.01 |
| 2 | 3.42 ± 0.01 | 6 | 4.26 ± 0.02 |
| 3 | 3.81 ± 0.01 | 7 | 5.10 ± 0.02 |
| 4 | 3.55 ± 0.01 | 8 | 4.99 ± 0.02 |

TABLE V. The crosstalk level of the silicon pad detector.

| channel | crosstalk(%) | crosstalk(%) | crosstalk(%) | crosstalk(%) |
|---|---|---|---|---|
| 1 | primary channel | 2.87±0.07 | 1.83±0.05 | 1.89±0.06 |
| 2 | 2.09±0.06 | primary channel | 2.05±0.06 | 2.00±0.06 |
| 3 | 2.00±0.06 | 2.98±0.08 | primary channel | 2.07±0.06 |
| 4 | 1.97±0.06 | 2.73±0.07 | 1.87±0.06 | primary channel |
| 5 | 1.80±0.05 | 2.59±0.07 | 1.72±0.05 | 1.62±0.05 |
| 6 | 0.34±0.04 | 1.31±0.05 | 0.28±0.04 | 0.19±0.04 |
| 7 | 0.49±0.05 | 1.36±0.06 | 0.17±0.05 | 0.19±0.05 |
| 8 | 0.47±0.05 | 1.48±0.06 | 0.28±0.04 | 0.19±0.04 |
| 1 | 1.89±0.06 | –0.75±0.04 | –0.59±0.03 | –0.47±0.03 |
| 2 | 1.99±0.06 | –0.58±0.03 | –0.43±0.03 | –0.29±0.03 |
| 3 | 1.91±0.06 | –0.81±0.04 | –0.67±0.04 | –0.57±0.04 |
| 4 | 1.75±0.05 | –0.84±0.04 | –0.71±0.04 | –0.64±0.03 |
| 5 | primary channel | –0.84±0.04 | –0.75±0.04 | –0.57±0.03 |
| 6 | 0.00±0.04 | primary channel | 2.73±0.08 | 2.80±0.08 |
| 7 | 0.03±0.05 | 2.69±0.08 | primary channel | 3.11±0.09 |
| 8 | 0.18±0.05 | 2.66±0.08 | 3.03±0.08 | primary channel |

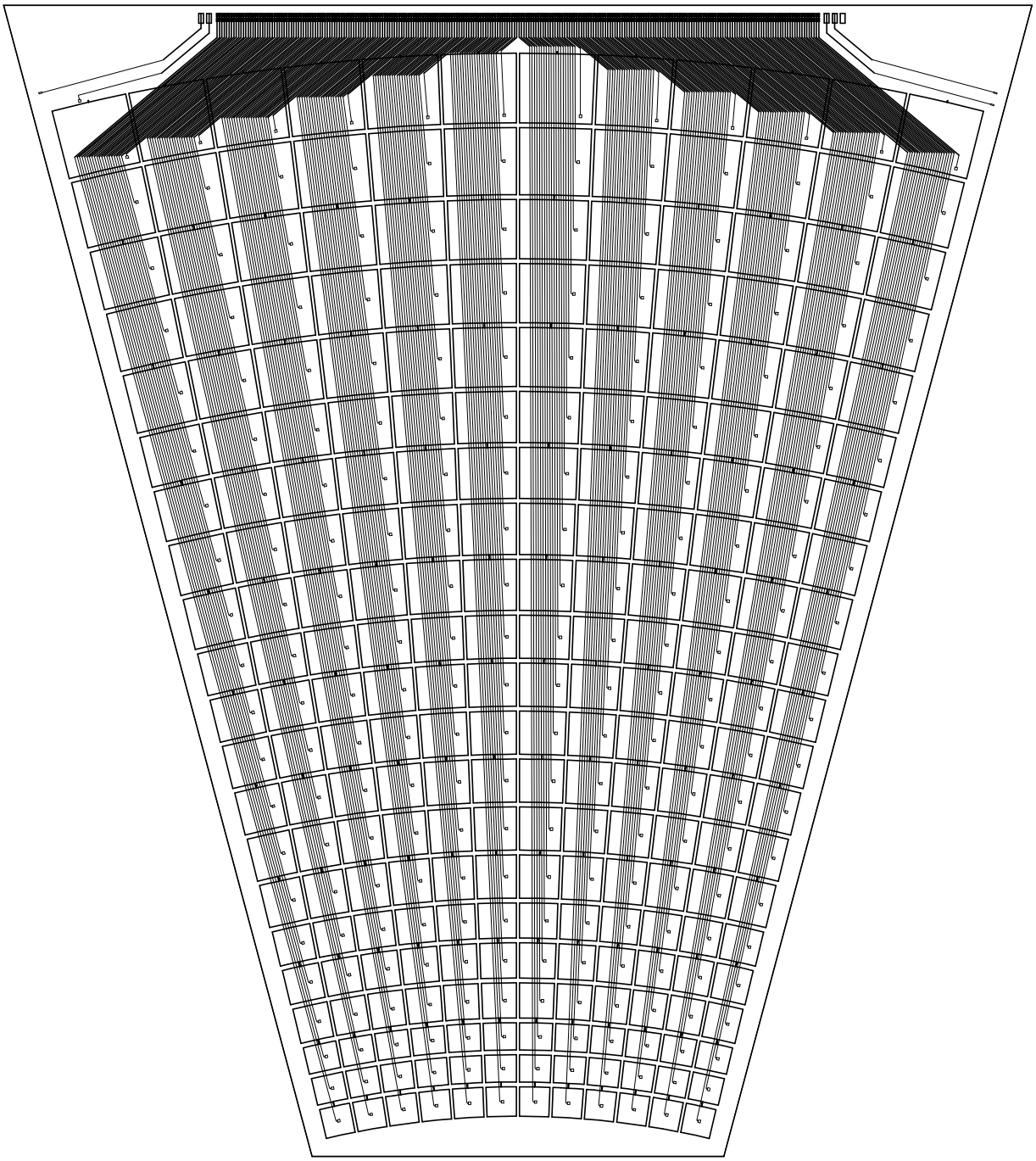

FIG. 1. Picture of the silicon pad detector for the PHENIX MVD "endcaps".

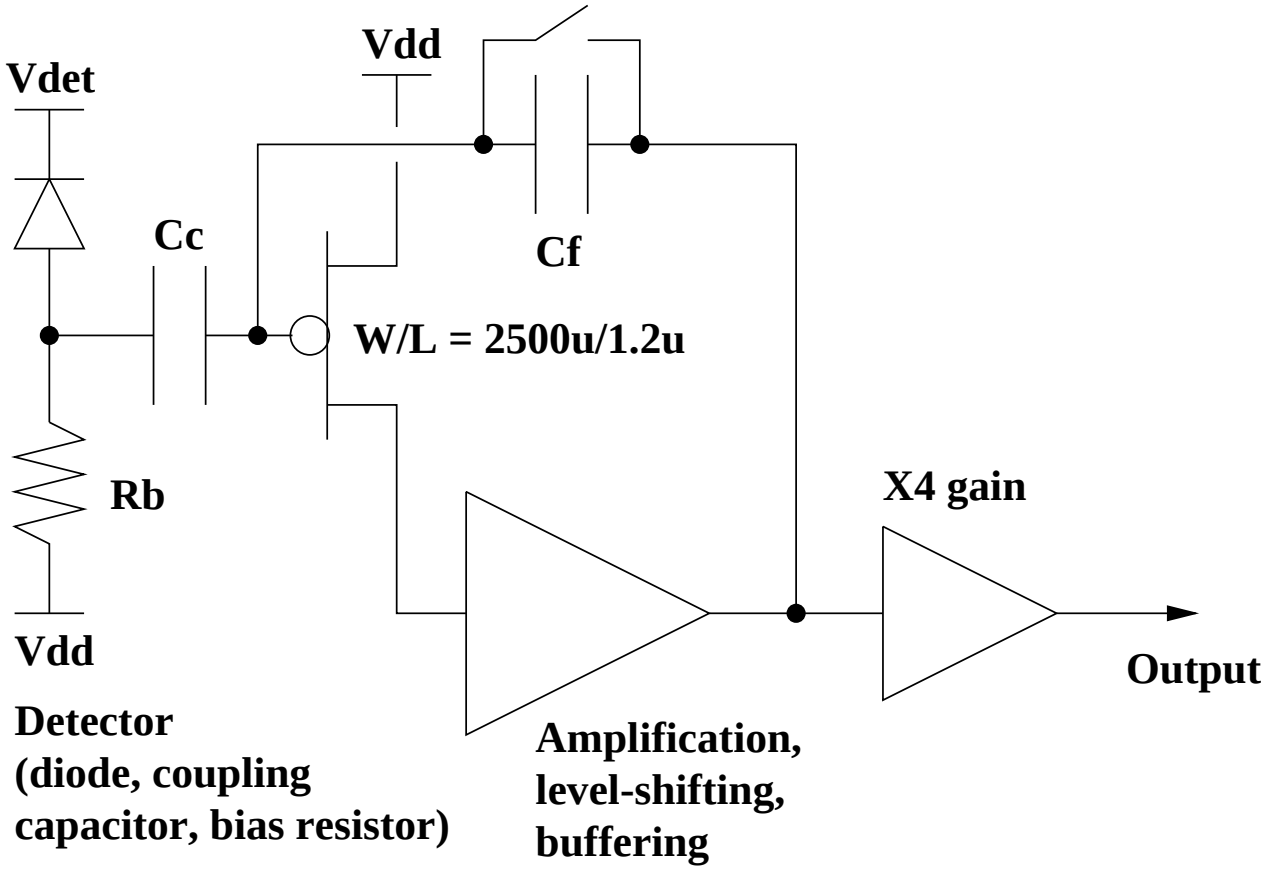


FIG. 2. Preamplifier and detector block diagram.

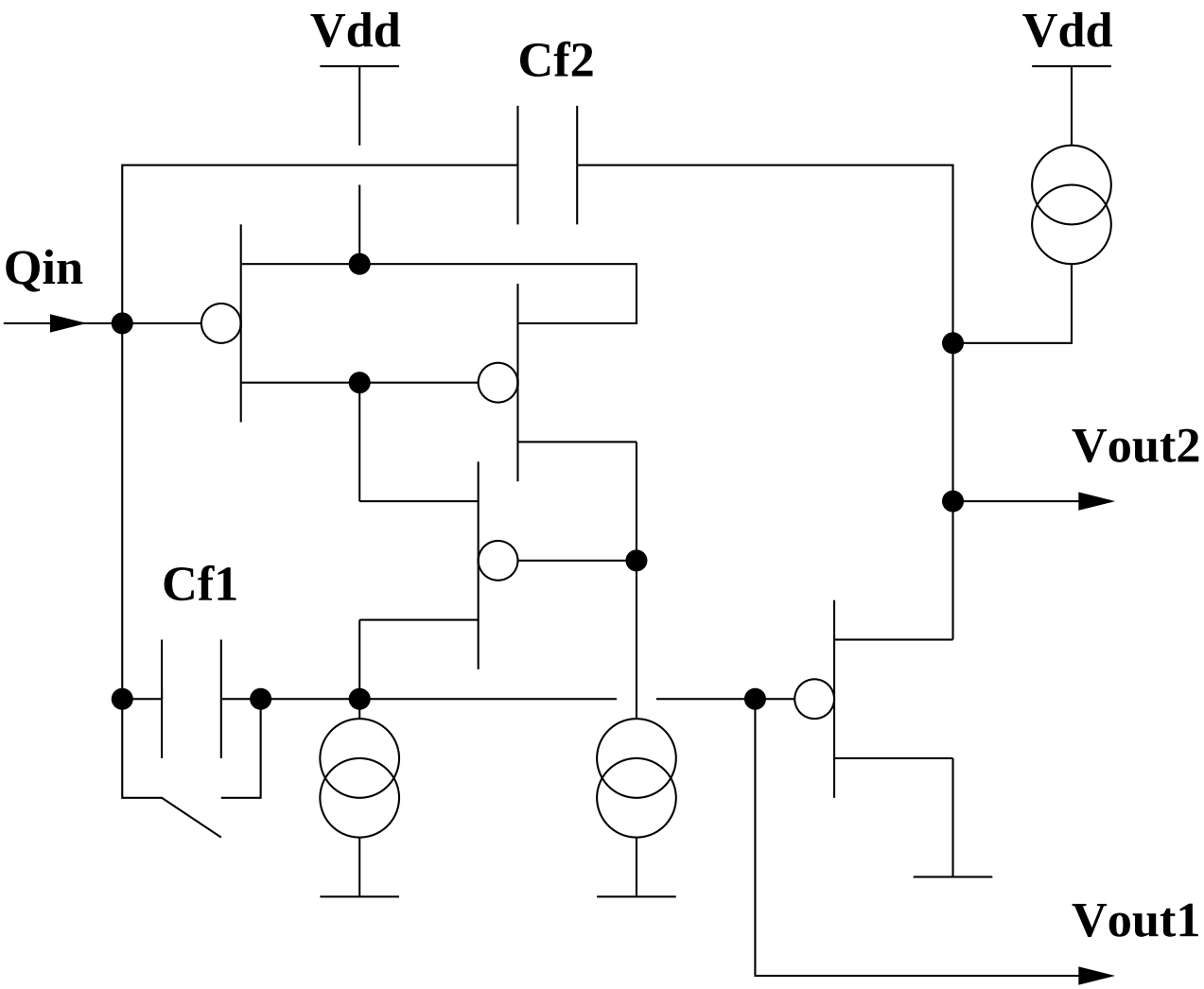


FIG. 3. Preamplifier detail.

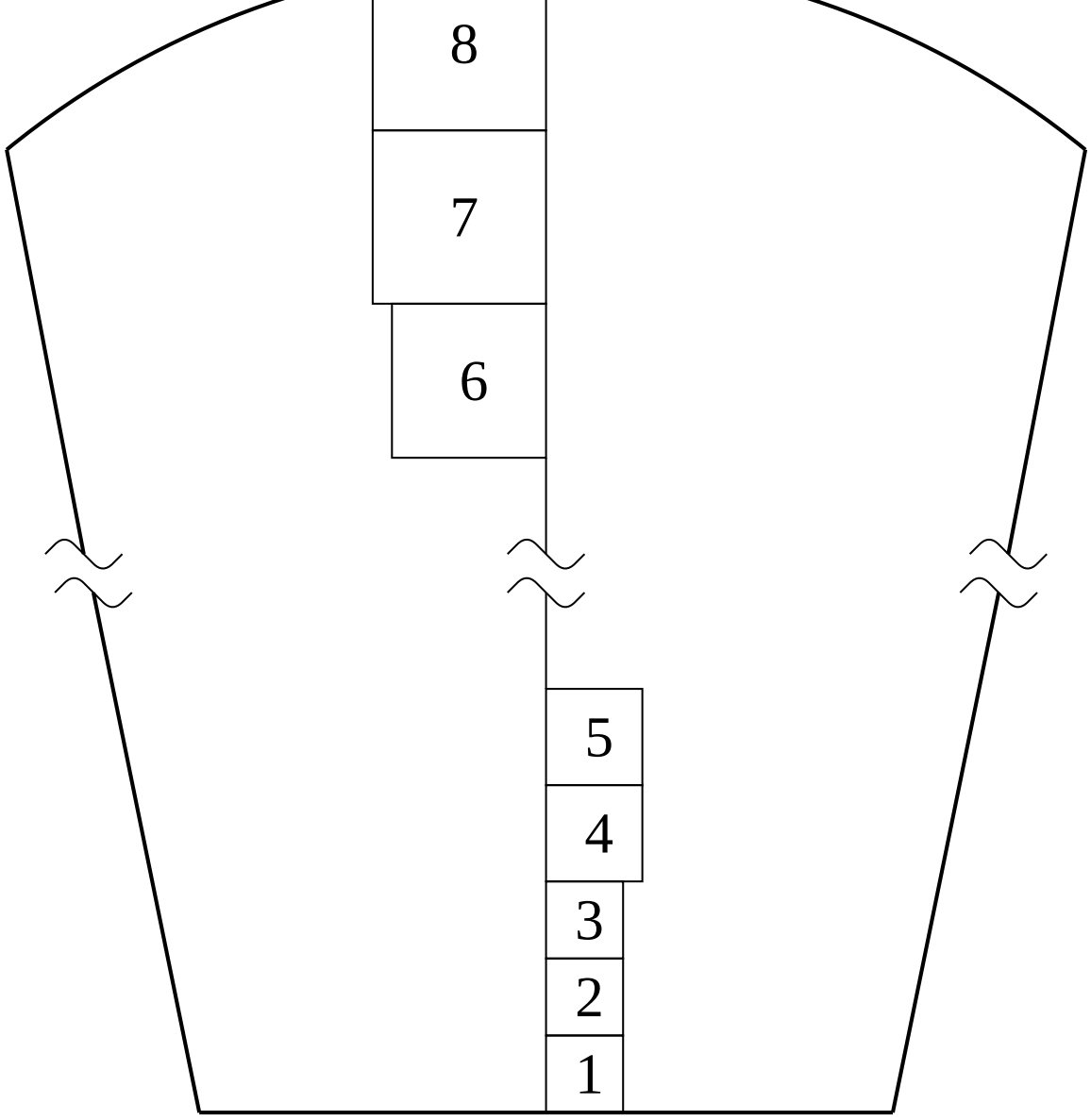


FIG. 4. The pad channel numbering convention in this test.

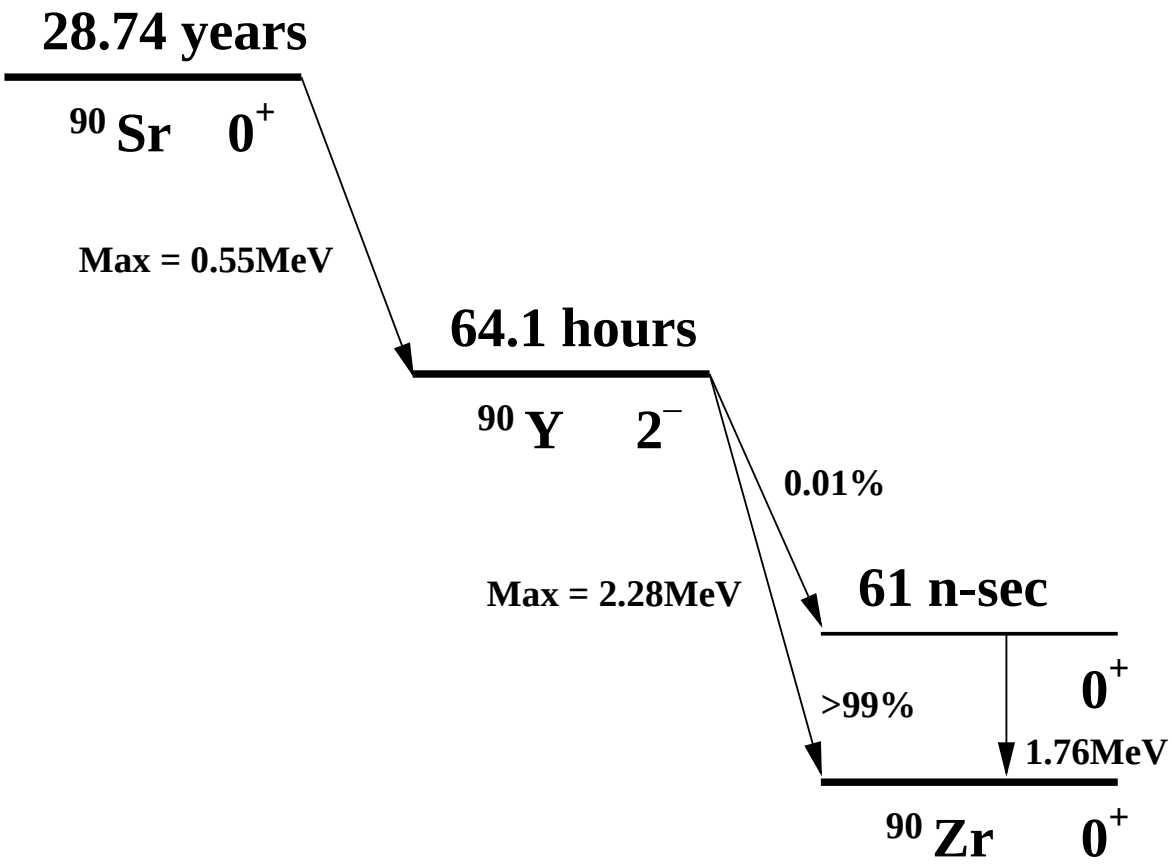


FIG. 5. The decay scheme of $^{90}$Sr.

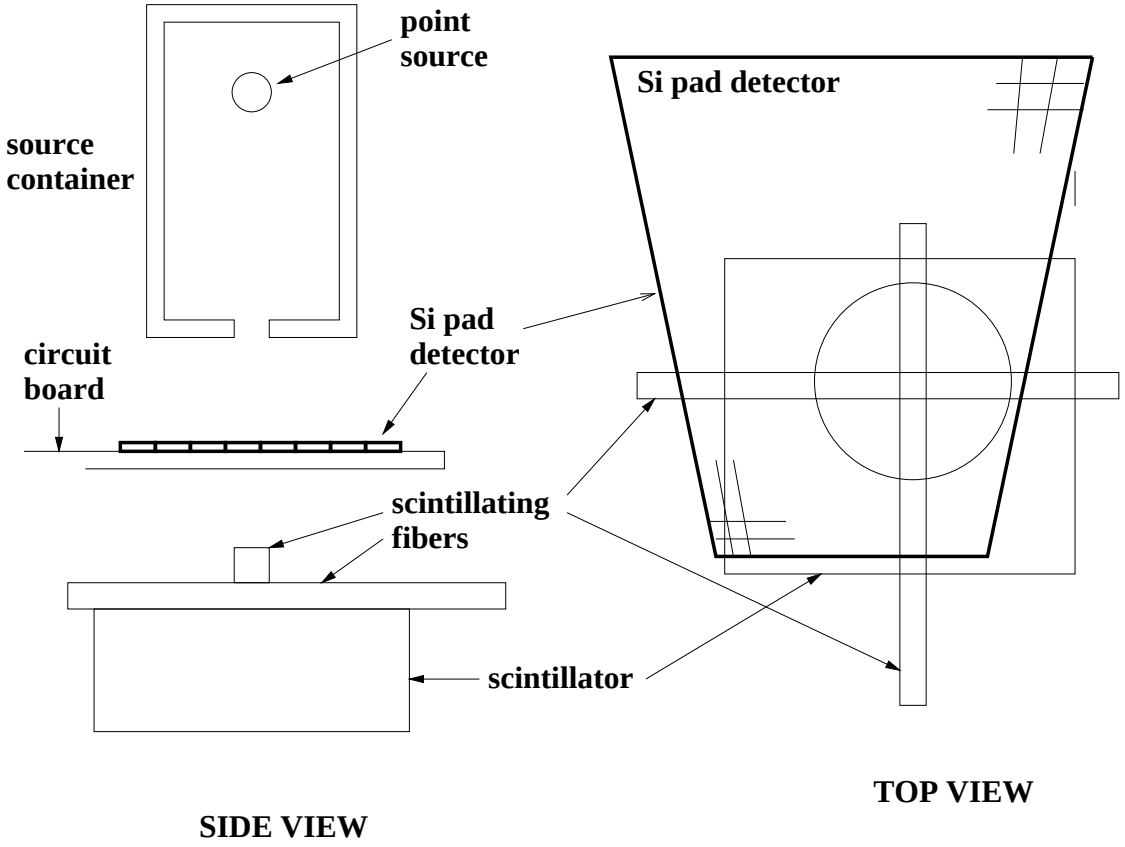


FIG. 6. The test stand geometry.

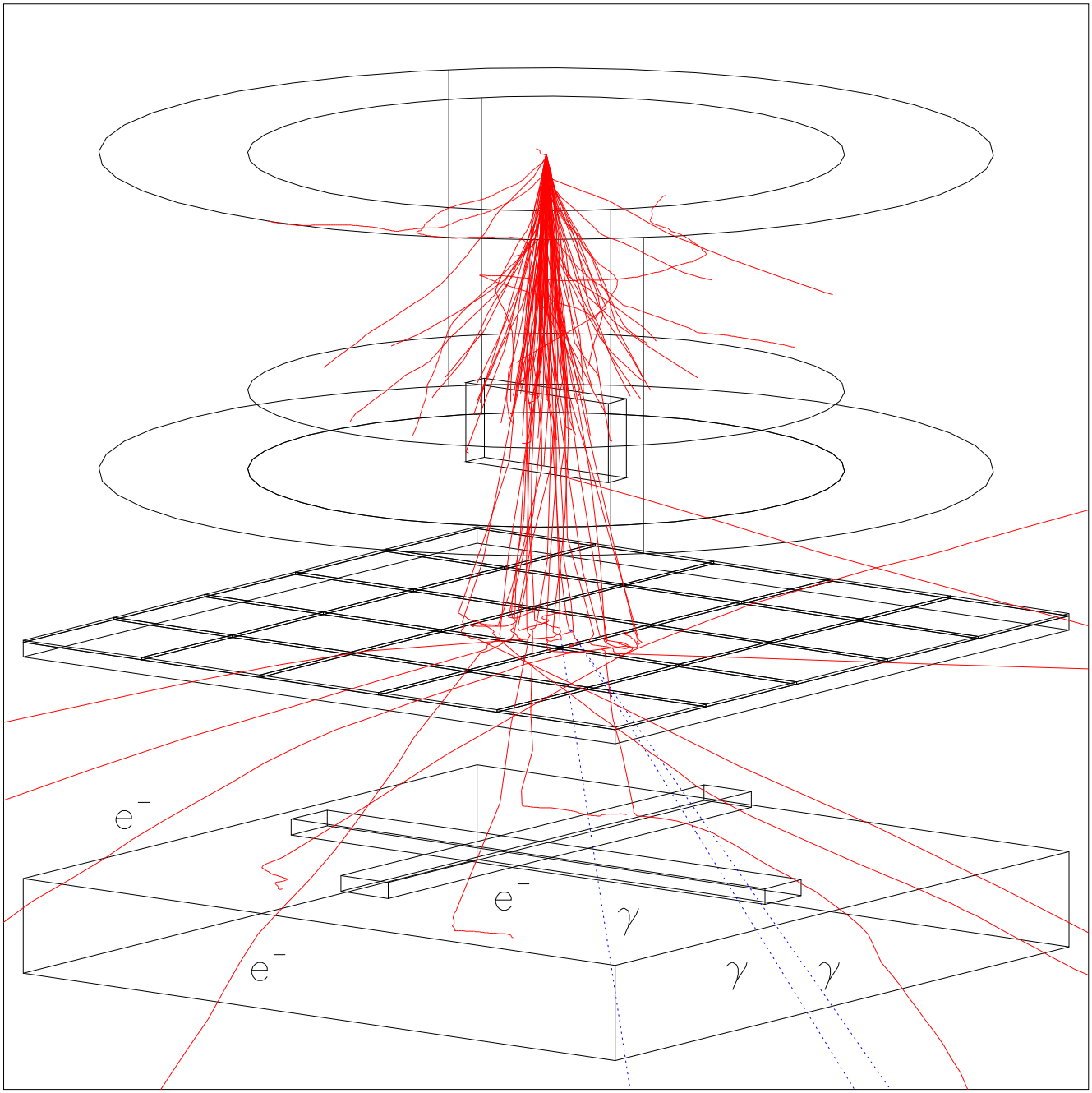


FIG. 7. An example of the Monte Carlo simulation. 100 electrons were generated in this sample. The solid lines represent the trajectories of electrons and dotted lines represent the secondary bremsstrahlung photons.

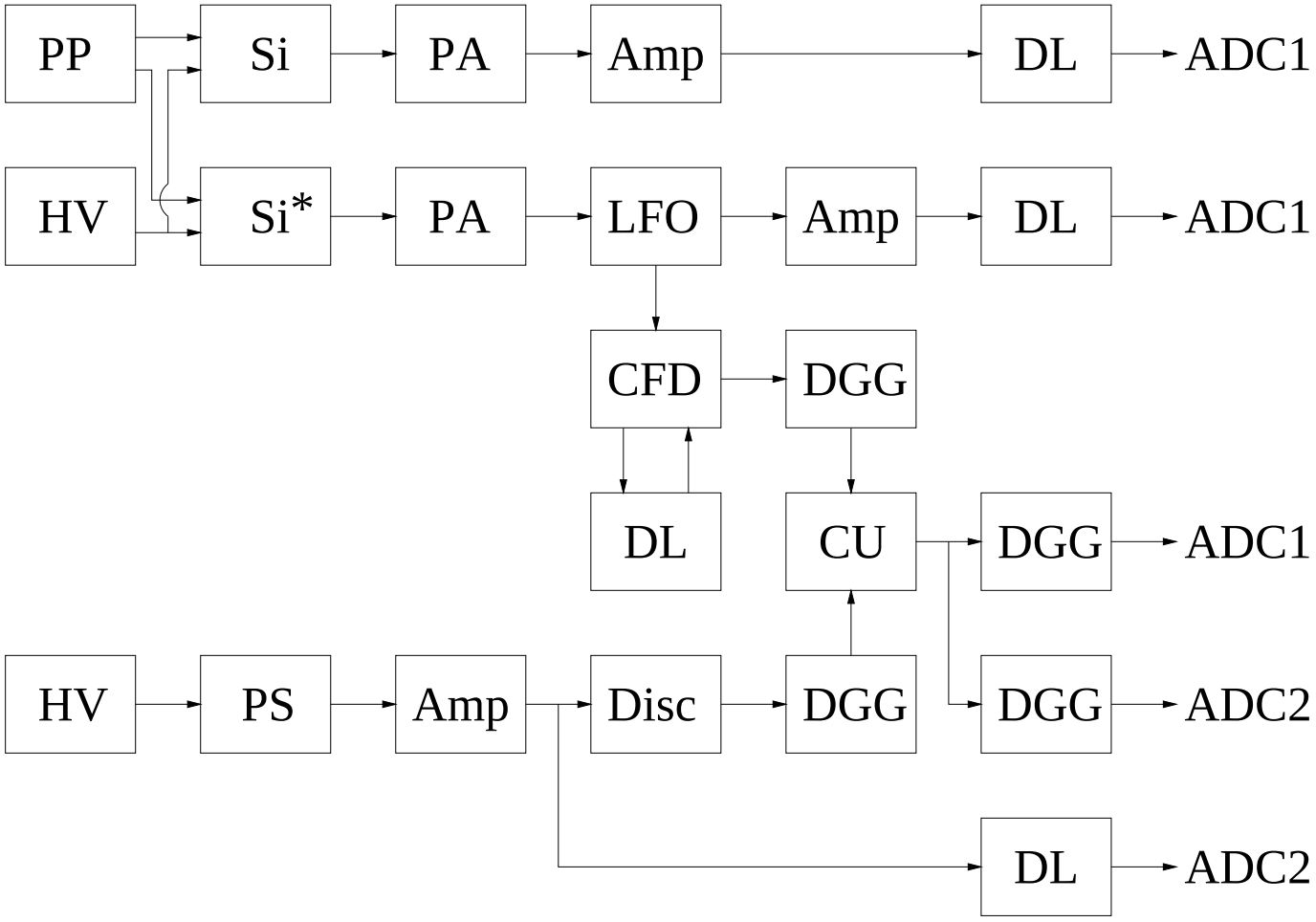


FIG. 8. The block diagram for the electronics used in the test. +30V bias voltage was supplied to the silicon pad detector. Si* represents the primary channel(channel illuminated by the source) and Si represents one of the neighboring channels. HV = high voltage supply, PP = preamplifier power supply, CFD = constant fraction discriminator, CU = coincidence unit, DL = delay line, PS = plastic scintillator, LFO = linear fan out, PA = preamplifier, and DGG = delay and gate generator.

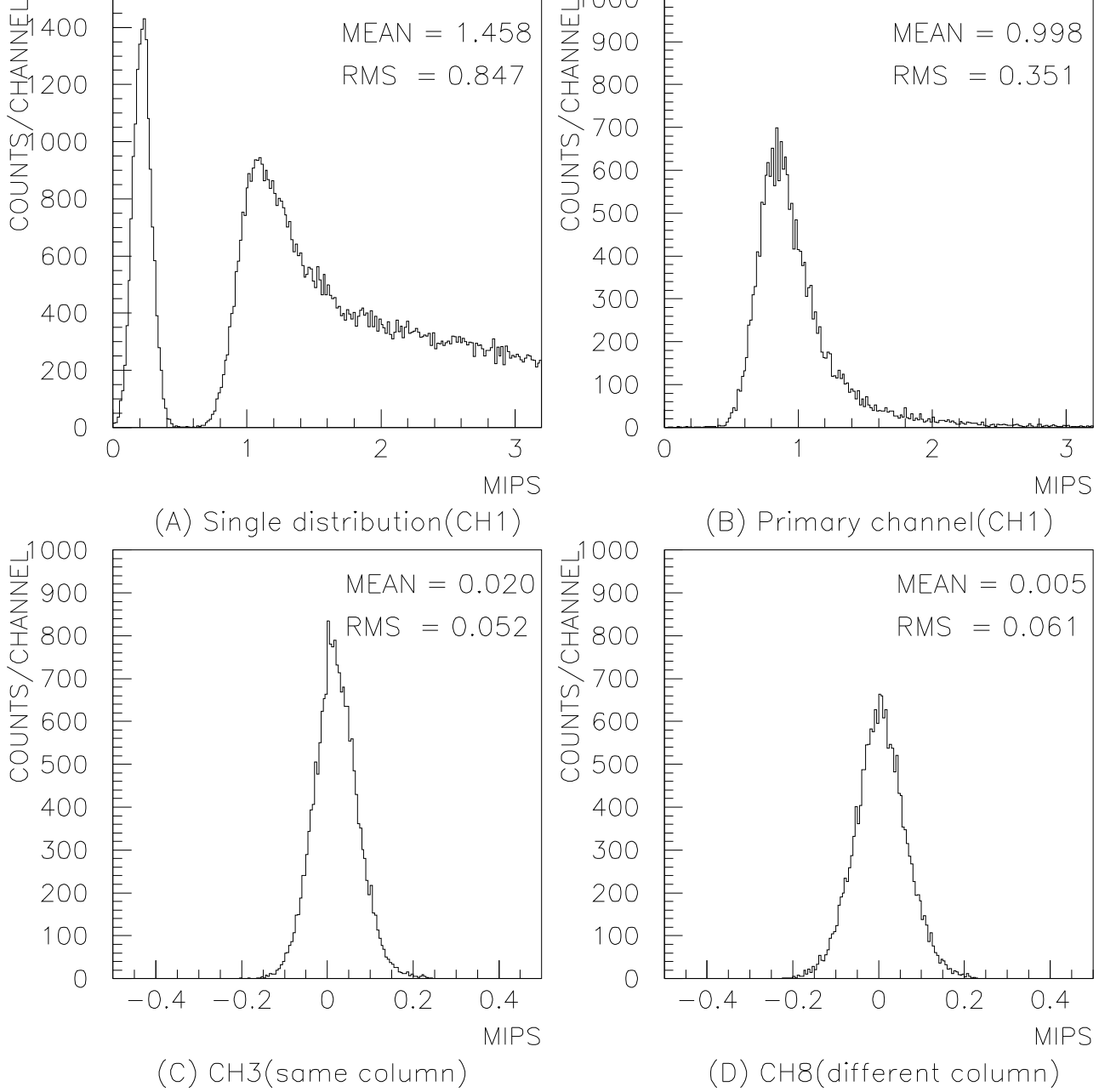


FIG. 9. The ADC distributions. (A)the single spectrum for the primary channel. (B)primary channel. (C)neighboring channel(in the same column). (D)neighboring channels(in the different column).

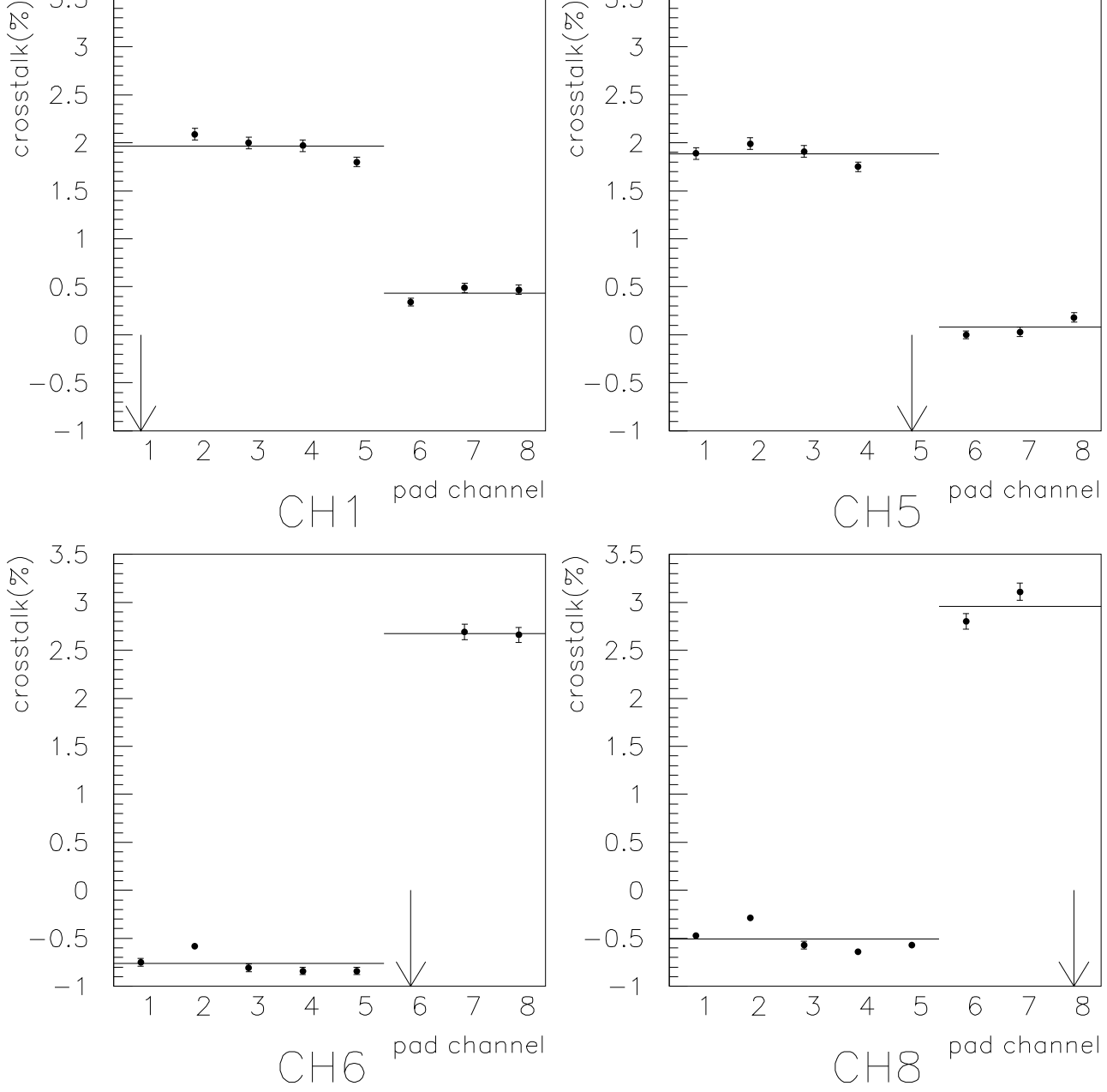


FIG. 10. The results of the crosstalk measurement. Arrows represent the channels illuminated by the source.